Dalton Transactions

Accepted Manuscript

ROYAL SOCIETY OF CHEMISTRY

www.rsc.org/dalton

Oxy-functionalization of Group 9 and 10 Transition Metal Methyl Ligands: Use of Pyridine-based Hemi-labile Ligands

Bruce M. Prince, T. Brent Gunnoe[∞,]*, Thomas R. Cundari*

Center for Catalytic Hydrocarbon Functionalization (CCHF), Department of Chemistry, Center for Advanced Scientific Computing and Modeling (CASCaM); University of North Texas, 1155 Union Circle, #305070, Denton, TX 76203-5017
[∞]Department of Chemistry, University of Virginia, Charlottesville, VA 22904

Abstract: Hemi-labile ligands (HLLs) are intriguing candidates for catalysts since they may facilitate bond activation and bond formation through facile ligand dissociation/association. DFT studies are reported of hemi-labile ligands in conjunction with Group 9 and 10 metals for oxygen atom insertion into metal-methyl bonds. Analysis of the reaction of pyridine-*N*-oxide with d^8-$[L_nM(Me)(THF)]^{q+}$ (M = Co, Rh, Ir, Ni, Pd, Pt; L_n = 2-(CH_3OCH_2)Py; q = 0 and +1 for Group 9 and 10 metals, respectively; Py = pyridine; THF = tetrahydrofuran) indicates that oxy-insertion for Group 9 complexes occurs with lower free energies barriers than their Group 10 congeners. Analysis of structural changes along the reaction coordinate suggests that the initial oxygen atom transfer and subsequent methyl migration steps are favored by a reduction and increase, respectively, in coordination number. This emphasizes that HLLs could be uniquely positioned to assist both transformations within a single complex. Additionally, such ligands are worthy of experimental study due to their ability to meet the disparate coordination demands for two-step, redox-based oxy-insertion.

Introduction

For selective partial oxidation of small alkanes, new and improved catalysts are needed to leverage the abundant natural gas reserves for use as liquid transportation fuels. For example, direct moderate temperature/pressure (≤ 250 ºC and 500 psi) oxidation of methane to methanol (MTM) has garnered substantial attention as an alternative to the syngas route.[1-3] For the partial oxidation of methane and other small alkanes, the inorganic and organometallic chemistry communities have extensively researched a variety of transition metals, ligand sets, and oxidants with the goal of active and long-lived catalysts that function at moderate conditions.[1-16]

There are two critical steps in catalytic methane functionalization: activation of the methane C–H bond and C–X (X = functional group such as halide or oxygen-based group) bond formation. Well-defined functionalization of methyl ligands is relatively rare and less well studied than C–H bond activation. Late transition metal catalysts that functionalize methane are proposed to mediate C–X bond formation via a reductive nucleophilic addition to an electrophilic methyl ligand.[5,9,12,15,17,18] An alternative route for C–O bond formation involves oxygen atom insertion into metal-methyl bonds; however, selective oxy-insertion into metal-hydrocarbyl bonds is rare.[14,17-24]

Our groups have modeled oxy-insertion via organometallic Baeyer-Villiger pathways including Pt^{II} complexes and a broad study of d^8 and d^6 complexes supported by bipyridyl ligands.[25,26] An important aspect of preparing viable candidates for metal-mediated oxy-insertion is an understanding of structure/activity relationships. A computational study focused on (bpy')Pt^{II} (bpy' = substituted bipyridine ligands) complexes indicated that organometallic Baeyer-Villiger oxy-insertion occurs with substantial (> 30 kcal/mol) barriers.[25] Subsequently, we studied the impact of metal identity on the activation barrier for oxy-insertion by a series of d^6 and d^8 complexes supported by bpy ligand(s).[25]

Given the few computational studies focused on oxy-insertion into metal-hydrocarbyl bonds,[14,24] there is a limited understanding of how various features of the supporting ligands influence the activation barrier. For example, investigations have shown that coordination number has a substantial effect on oxy-insertion activation barriers, Figure 2, and hemi-labile ligands (HLL) could allow facile access to low coordinate intermediates.[27-31] Herein, we report a modeling study of oxy-insertion into d^8-M–methyl bonds with hemi-labile pyridyl-ether ligands. The role of the hemi-labile pendant arm is proposed to help stabilize the metal complex during the oxy-insertion. While the pendant arm stayed within the coordination sphere, the computed structural evidence indicates that it partially dissociated from the metal center during the initial oxygen atom transfer and partially reassociated during the subsequent methyl migration, and thus facilitated the two-step oxy-insertion. Despite efforts to develop catalytic hydrocarbon partial oxidation and examples of stoichiometric O insertion into M–R bonds and 1,2-CH-addition across M–OR bonds,[26,32] no examples of a catalytic processes via this pathway has been reported.[16] Thus, developing a better understanding of how to design complexes that mediate both O atom insertion and C–H activation is critical to new catalyst design.

Computational Methods

The level of theory employed is density functional theory (DFT) within the Gaussian 09 package[33] to study the stationary points and the energetics for oxy-insertion pathways involving HLL complexes. The hybrid Becke 3-parameter (B3) functional with the Lee-Yang-Parr (LYP) exchange-correlation functional (*i.e.*, B3LYP[34-36]) was used along with a pseudopotential valence double-ζ basis set with d-polarization functions added to the main group elements (CEP-31G (d)). All quoted energies are free energies calculated at 298.15 K and 1 atm and utilize unscaled B3LYP/CEP-31G(d)[34,35,37] vibrational frequencies; continuum solvent effects (THF, ε = 7.4257) are modeled in the calculations using the CPCM formalism.[38] The present DFT calculations use tight convergence criteria and a larger grid for numerical integration.

Stationary points are characterized in the gas phase as minima or transition states (TSs) via calculation of the energy Hessian and observation of the correct number of imaginary frequencies, zero (0) and (1), respectively. To authenticate the imaginary modes, intrinsic reaction coordinates (IRC) are calculated from TS geometries. All geometry optimizations are performed without symmetry or coordinate restraint, and all species are singlets unless stated otherwise for which a restricted Kohn-Sham formalism is employed.

Results and Discussion

The HLL models studied here form a five-membered, bidentate N~O chelate ring upon coordination and possess ether or ester functionality as the hemi-labile "O-arm." Preliminary modeling suggested little difference between the ester and ether groups. Herein, we focused discussion on the ether arm. The less-labile portion of the HLL is a pyridine ligand ("N" in Scheme 1). Experimentally reported complexes motivated the present choices for the labile "arm" and non-labile portion of the HLL model complexes.[29,39-41]

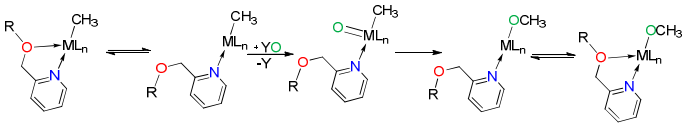

Scheme 1. Metal-mediated oxy-insertion reaction scheme involving a hemi-labile ligand ($PyCH_2OR$), YO = oxidant, Y = leaving group, and R = alkyl.

A one-step (non-redox) Baeyer-Villiger (BV) type pathway (red) was initially explored given its precedent for several d^0 complexes, Scheme 2.[18,42,43] For complexes studied herein, the BV mechanism is calculated to involve a much higher barrier than the alternative two-step, oxo-mediated (or redox) pathway (black, Scheme 2). Thus, the discussion in this paper is focused on the metal-oxo mediated pathway for oxy-insertion into a metal-methyl bond.

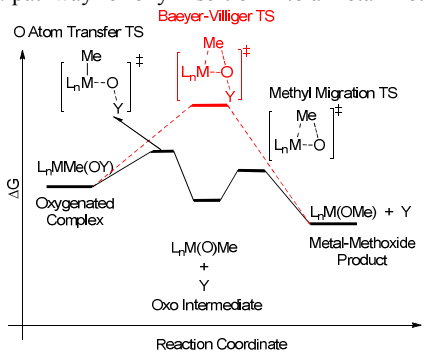

Scheme 2. Proposed pathways for reaction of L_nM–Me + YO leading to the production of $L_nM(OMe)$ + Y. YO = Oxidant.

Our main goal is to use theory to assess the feasibility of HLL complexes for the oxy-insertion step for group 9 and 10 methyl complexes with d^8 electronic configurations. This paper focuses on (i) comparison of Group 9 and 10 metals, (ii) assessing the coordination environment of the metal center, (iii) competing pathways (*e.g.*, associative *vs.* dissociative), and (iv) the role of N~O hemi-lability in the two steps (*i.e.,* oxo formation and methyl migration to the oxo ligand).

1. Redox Pathway of HLL

In our model studies, pyridine-*N*-oxide (PyO) coordinates to a methyl complex followed by O atom transfer and pyridine dissociation to form an oxo (O in Scheme 1) intermediate. Subsequent pyridine (re)coordination to the metal may occur. Additionally, the various stationary points in the oxy-insertion reaction coordinates can have the hemi-labile arm totally or partially dissociated or associated. Formation of an oxo-methyl intermediate is followed by C–O bond formation via methyl migration to the oxo ligand to give a methoxide complex. For a complete MTM catalytic cycle, methane C–H bond activation would take place across the M–OMe bond to produce the methanol product and M–Me. Preliminary results confirmed dissociation of the ether arm assists the formation of the oxo intermediate, while association of the ether arm assists the subsequent methyl migration step (Scheme 2). The latter will be discussed in more detail in the section 4.

2. Group 10 Complexes

2.1. Platinum

A computed free energy surface for oxy-insertion involving a cationic-Pt^{II}-HLL complex is shown in Scheme 3, and pertinent stationary point geometries are shown in Figure 1; those for Ni^{II}, Pd^{II}, Co^{I}, Rh^{I}, Ir^{I} metals are qualitatively similar and the requisite data are collected in Supporting Information. Displacement of THF by PyO leading to formation of the $[(N\sim O)Pt(OPy)(Me)]^+$ is calculated to be exergonic by -12.4 kcal/mol. For both the THF-ligated precursor and $[(N\sim O)Pt(OPy)(Me)]^+$, Pt is weakly bonded to the pendant ether arm. In both cases, the calculated Pt^{II}–O_{ether} bond distance is ~2.3 Å, which is long compared to bond distances between 2.07 and 2.23 Å for the five experimental examples of four-coordinate Pt^{II}-ether complexes in the Cambridge Structural Database.[44-47] The barrier for rate-determining step (RDS) oxygen atom transfer (OAT) to form a Pt^{IV}-oxo $\{[N\sim O)Pt^{IV}(Py)(O)(Me)]^+$ via transition state **OAT**‡ is very large, $\Delta G^{‡}$ = 49.3 kcal/mol (Scheme 3). Two pathways were isolated computationally from $[(N\sim O)Pt(OPy)(Me)]^+$, one in which the Py (from the oxidant, OPy) remains coordinated to the metal and one in which it does not. The five-coordinate (Py-ligated) pathway is substantially lower in free energy than the four-coordinate (Py-free) pathway (Scheme 3). The last step of the oxy-insertion process, methyl migration, proceeds via transition state **MeMig**‡, which results in the Pt^{II}-methoxide complexes $[(N\sim O)Pt(Py)(OMe)]^+$ and $[(N\sim O)Pt(OMe)]^+$ from the Pt^{IV}-oxo/methyl intermediates. The barrier for the methyl migration transition state of the five-coordinate complex, is found to be lower (ΔG = 25.8 kcal/mol) by 24.3 kcal/mol when compared to the four-coordinate complex (Scheme 3).

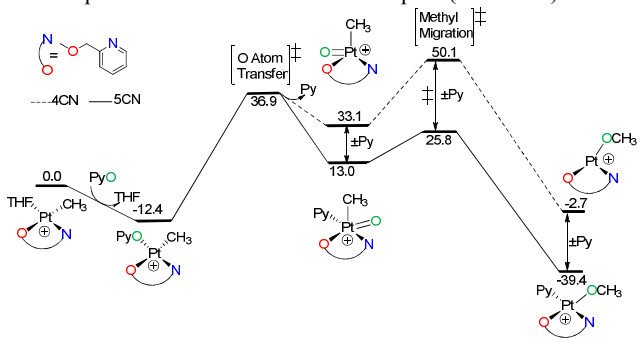

Scheme 3. B3LYP/CEP-31G(d) calculated free energies (in kcal/mol relative to $[(N\sim O)Pt^{II}(THF)(Me)]^+$ + PyO) for oxy-insertion with a cationic HLL-Pt^{II} complex for four- and five-coordinate intermediates.

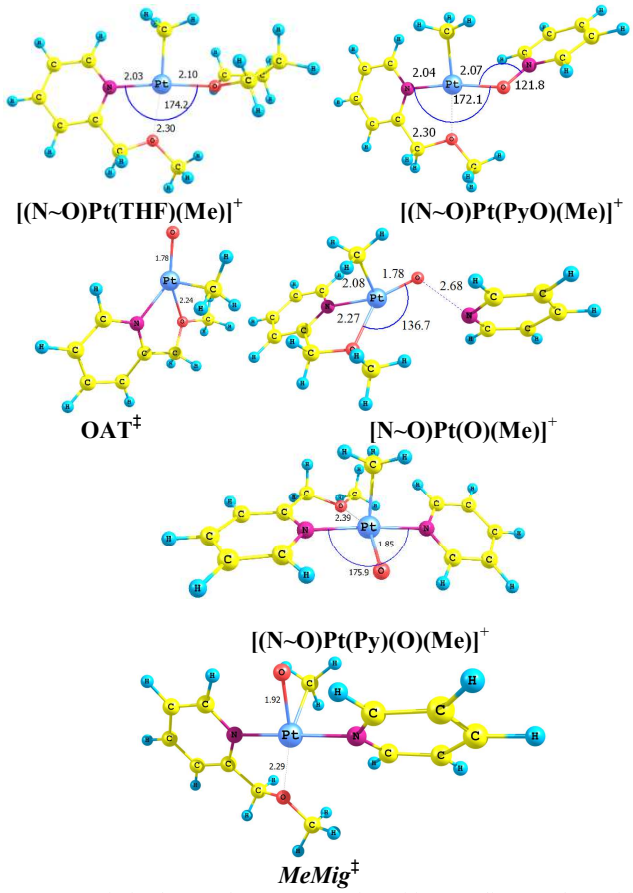

Figure 1. Optimized ground state geometries of intermediates and transition states for oxy-insertion by complex $[(N\sim O)Pt(THF)(Me)]^+$ and pyridine-*N*-oxide (PyO). Bond lengths and bond angles are in Å and °, respectively.

2.2. Nickel and Palladium

The reaction coordinate for oxy-insertion using Pt^{II} (Scheme 3) was compared to its 3d congener nickel (Scheme 4). The O-atom transfer (OAT) barrier from $[(N\sim O)Ni(OPy)(Me)]^+$ is calculated to be 45.7 kcal/mol, and formation of the five-coordinate Ni-oxo intermediate $[(N\sim O)Ni(Py)(O)(Me)]^+$ is endergonic (+15.6 kcal/mol) relative to starting materials (Scheme 4). The lower OAT barrier for Ni relative to Pt (calculated $\Delta\Delta G^{\ddagger}$ =4.0 kcal/mol) may be ascribed to the favorable hard acid/hard base interactions between oxygen and nickel.[48] The large calculated $\Delta G^{\ddagger}$ for the O atom transfer suggests an unfavorable oxy-insertion for this and related Ni complexes when using OPy as oxidant. Previous computational research on Ni^{II}–R complexes suggests that more potent oxidants such as N_2O are needed for oxy-insertion into Ni-carbon bonds,[49] which is supported by experiment.[50-53] Note that in the cases modeled here that methyl migration to form methoxy complex has a lower barrier than the initial O atom transfer to make the oxo.

The Pt^{II}-HLL complex was also compared to its 4d congener palladium (Scheme 4). Previously reported O atom insertions into Pd–R bonds have been suggested to occur via Pd-oxo intermediates (although there is no evidence for the intermediacy of Pd-oxo species).[54,55] The O-atom transfer barrier from $[(N\sim O)Pd(OPy)(Me)]^+$ is calculated to be 59.8 kcal/mol, while the five-coordinate oxo intermediate is 26.4 kcal/mol endergonic relative to starting materials (Scheme 4). The higher O atom transfer free energy barrier and more unstable oxo intermediate for Pd relative to Pt may arise from the greater instability of the +4 formal oxidation state for Pd versus Pt.

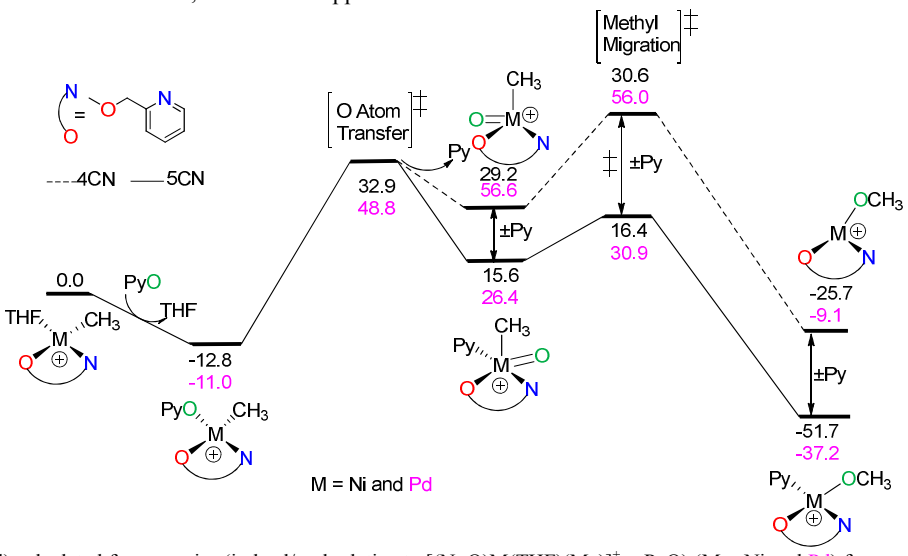

Scheme 4. B3LYP/CEP-31G(d) calculated free energies (in kcal/mol relative to $[(N\sim O)M(THF)(Me)]^+$ + PyO) (M = Ni and Pd) for oxy-insertion with a cationic HLL-M^{II} complex for four and five coordinate species.

3. Group 9 Complexes

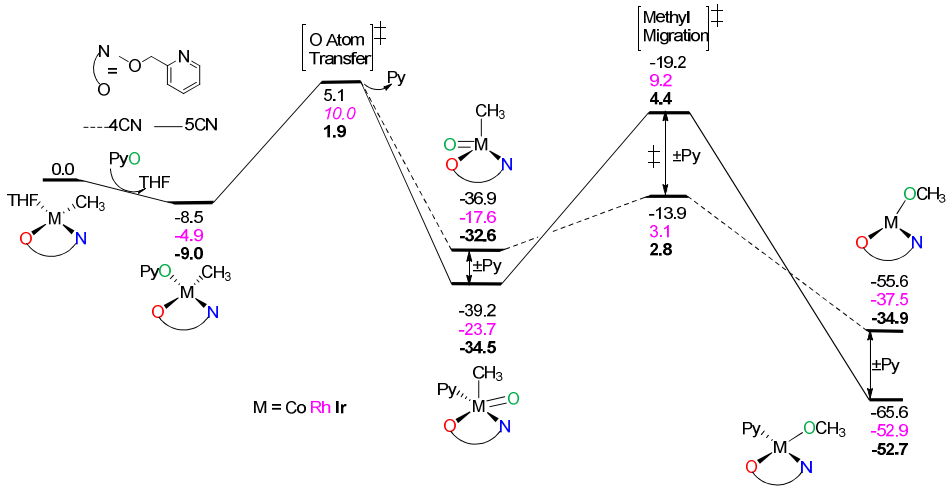

Scheme 5. B3LYP/CEP-31G(d) calculated free energies (in kcal/mol relative to (N~O)M(THF)(Me) (M = Co, Rh or **Ir**) for oxy-insertion with charge neutral HLL-M^{I} complexes for four- and five-coordinate species.

Relative to the THF-ligated precursor, the Co-oxo free energies are calculated to be very stable, ΔG = -36.9 and -39.2 kcal/mol for the four- and five-coordinate model complexes, respectively. The calculated O atom transfer barrier from (N~O)Co(OPy)(Me) is only 13.6 kcal/mol (Scheme 5). Thus, in comparison to the cationic group analog $[(N\sim O)Ni(OPy)(Me)]^+$, the formation of the Co-oxo intermediate has a large 32.1 kcal/mol advantage in the calculated $\Delta\Delta G^{\ddagger}$. The methyl migration transition state is calculated to be 20.0 kcal/mol relative to oxo complex for the lower energy five-coordinate pathway. From a kinetic and thermodynamic viewpoint, the calculations suggest that this neutral Group 9 complex is more promising than its cationic Group 10 congener (M = Ni, Scheme 4) for oxy-insertion into M–Me bonds. The four-and five-coordinate Ir-oxo intermediates lie in a thermodynamic sink with ΔG = -32.6 and -34.5 kcal/mol, respectively. The O atom transfer barrier is only 10.9 kcal/mol relative to the pyridine-*N*-oxide adduct, while the methyl migration free energy barrier is computed to be 35.4 and 38.9

kcal/mol relative to the oxo intermediate, respectively (Scheme 5), substantially higher than the Co and Rh (*vide infra*) models. Unlike other systems discussed thus far, both the four- and five-coordinate methyl migration is predicted to be disfavored ($\Delta G^{\ddagger}$) ~37.0 kcal/mol relative to the Ir-oxo, which may suggest that the Ir-oxo intermediate is highly unstable in comparison to its congeners.

Conversion of the THF-bound Rh^{I} precursor [(N~O)Rh(THF)(Me)] to the Rh-oxo complexes (N~O)Rh(O)(Me) and (N~O)Rh(O)(Py)(Me) is calculated to be exergonic with ΔG = -17.6 and -23.7 kcal/mol for the four- and five-coordinate intermediates, respectively. The calculated O atom transfer barrier ($\Delta G^{\ddagger}$) is 15.0 kcal/mol (Scheme 5), only 1.3 kcal/mol higher than calculated for the Co congener. Methyl migration barriers for four- and five-coordinate pathways are both 26.8 kcal/mol relative to the corresponding oxo. As with the Co/Ni pair, calculations suggest that this neutral Group 9 complex is kinetically and thermodynamically more promising than its cationic Group 10 congener Pd.

4. Influence of Hemi-Labile Ligand

The DFT calculated structures show that the HLL ligand forms distinctive bonds to the metals: one via the pyridine functionality and the other involving the potentially hemi-labile ether arm. Importantly, the latter of these bonds changes along the reaction coordinate for oxy-insertion. It was initially conjectured that the ether arm of 2-(CH_3OCH_2)Py could display variable binding to the central metal via what may be visualized as on-off or "windshield wiper" effect during the oxy-insertion reaction coordinate. The M–O_{ether} bond lengths (M–N_{py} distances change much less along the reaction coordinate) are plotted in Figure 2 and support this hypothesis. The general rise in the M–O_{ether} bond lengths by ~0.1 to 0.2 Å from the OPy adducts $[(N\sim O)M(OPy)(Me)]^{n+}$ (n = 0 or 1) to the oxo intermediates $[(N\sim O)M(O)(Py)(Me)]^{n+}$ (Figure 2) is in contrast to the reduction in bond length that might be expected based on an increase in the central metal's formal oxidation state. The expansion of M–O_{ether} bond lengths as O atom transfer occurs is consistent with the hypothesis that the HLL assists the formation of the oxo complex through partial dissociation of the ether arm. The M–O_{ether} bond lengths generally contract during the methyl migration, which once again overrides the change expected from formal oxidation state variations as the metal is reduced from the M^{q+2}-oxo intermediate to the M^{q+}-methoxide complex during the methyl migration step.

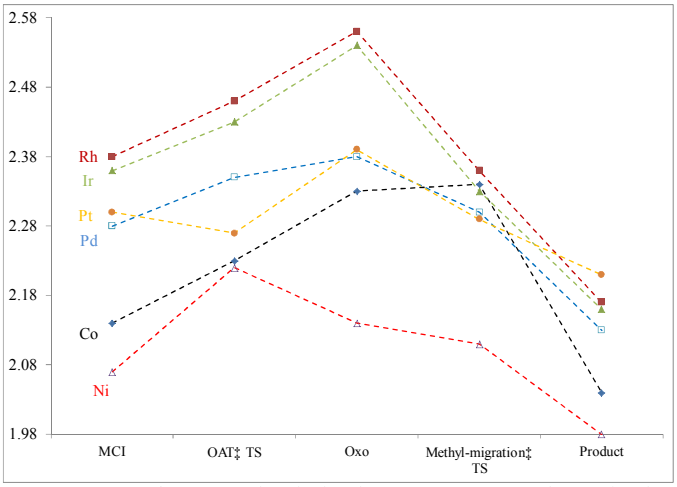

Figure 2. B3LYP/CEP-31G(d) calculated M–O_{ether} (M = Co, Rh, Ir, Ni, Pd or Pt) bond lengths (x-axis, Å) for hemi-labile ligand along lowest free energy oxy-insertion reaction coordinate (y-axis) for Group 9 and 10 complexes. All species possess formally d^8 metal ions, except for the d^6-oxo intermediates.

Distinctions are seen in the above generalizations about changes in M–O_{ether} bond lengths (Figure 2), most notably for the 3d metals Co and Ni. This indicates that the hemi-lability of 2-(CH_3OCH_2)Py is to some extent also metal-dependent. However, Figure 2 provides support for the "windshield wiper" effect, whereby the ether arm of the hemi-labile ligand may partially dissociate/associate, to assist the disparate electronic and steric demands of the initial oxidation and subsequent reduction steps of two-step, oxo-mediated oxy-insertion.

5. Summary, Conclusions and Prospectus

The current research explores the potential of hemi-labile ligands in conjunction with Group 9 and 10 metals for oxy-insertion into metal-methyl bonds. The results of DFT calculations support the proposal that the hemi-lability of 2-(CH_3OCH_2)Py may facilitate the desired two-step oxy-insertion reaction for metal-methyl bonds by the partial dissociation and re-association of the ether arm to the metal center during the initial oxo formation and subsequent methyl migration steps, respectively. Several additional important conclusions have resulted that can inform synthetic attempts to identify Group 9 and 10 transition metal complexes with HLL supporting ligands for which oxy-insertion is facile. Table 1 collects the relevant free energies.

Table 1. Relative Free Energies (B3LYP/CEP-31G(d), STP, kcal/mol) for Group 9 and 10 Complexes.

Metal[a]	$\Delta G_{oxo}^{\ddagger}$	ΔG_{oxo}	$\Delta G_{mig}^{\ddagger}$
Ni^+	45.6	15.6	0.7
Pd^+	59.8	26.4	4.5
Pt^+	49.3	13.0	12.8
Co	13.5	-39.2	20.0
Rh	15.0	-23.7	26.8
Ir	10.9	-34.5	31.7

[a] The superscript $^+$ denotes cationic complexes; the remainder are neutral. All reactants and final products are d^8 with formally d^6-oxo intermediates.

For cationic Group 10 complexes, the calculated barrier to formation of the oxo intermediate ($\Delta G_{oxo}^{\ddagger}$, Table 1) is quite large, > 40 kcal/mol, suggesting that oxo intermediates will be kinetically inaccessible at reasonable temperatures. Thus, the simulations suggest that stronger YO would need to be employed to observe O atom insertion for the cationic Group 10 complexes, but such high energy oxidants, which likely could not be recycled from dioxygen, would be impractical for large scale alkane oxidation reactions.[11] For neutral Group 9 complexes, in contrast, the barriers to formation of the oxo intermediates are ≤ 15 kcal/mol, Table 1. For the Co, Rh and Ir models the calculations indicate that the oxo intermediates lay in a thermodynamic "sink" (see ΔG_{oxo} in Table 1). The DFT results for the neutral Rh complex seem most promising among systems studied here. The Rh-oxo is in less of a thermodynamic sink than its 3d and 5d neighbors, while the methyl migration barrier ($\Delta G_{mig}^{\ddagger}$, Table 1) is still computed to be reasonable at 26.8 kcal/mol. Moving forward, identification of non-labile portions of HLLs, for example, replacement of pyridine and related imine ligands with N-heterocyclic carbenes, that can maintain reasonable O atom transfer barriers, that are not prone to oxidation, and that remove the oxo intermediate from its thermodynamic sink would appear worthy of scrutiny. Finally, among the d^8 model complexes investigated here, neutral Group 9 entities appear to be the most promising synthetic targets. Experiments are now underway to realize these computational predictions.

Supporting Information Available: Cartesian coordinates of all calculated species and a full citation for reference 33. This material is available free of charge via the Internet.

Acknowledgement: This work was solely supported by the Center for Catalytic Hydrocarbon Functionalization (CCHF), an Energy Frontier Research Center (EFRC) funded by the U.S. Department of Energy (DOE), Office of Science, Office of Basic Energy Sciences under Award Number DE-SC0001298.

References

(1) Crabtree, R. H. *J. Chem. Soc., Dalton Trans.* **2001**, 2437-2450.
(2) Hashiguchi, B. G.; Bischof, S. M.; Konnick, M. M.; Periana, R. A. *Acc. Chem. Res.* **2012**, *45*, 885-898.
(3) Olah, G. A. *Acc. Chem. Res.* **1987**, *20*, 422-428.
(4) Xu, X.; Kua, J.; Periana, R. A.; Goddard, W. A. *Organometallics* **2003**, *22*, 2057-2068.
(5) Gilbert, T. M.; Hristov, I.; Ziegler, T. *Organometallics* **2001**, *20*, 1183-1189.
(6) Horvath, I. T.; Cook, R. A.; Millar, J. M.; Kiss, G. *Organometallics* **1993**, *12*, 8-10.
(7) Sommer, J.; Bukala, J. *Acc. Chem. Res.* **1993**, *26*, 370-376.
(8) Sen, A. *Acc. Chem. Res.* **1988**, *21*, 421-428.
(9) Periana, R. A.; Bhalla, G.; Tenn III, W. J.; Young, K. J. H.; Liu, X. Y.; Mironov, O.; Jones, C.; Ziatdinov, V. R. *J. Mol. Catal. A: Chem.* **2004**, *220*, 7-25.
(10) Crabtree, R. H. *J. Organomet. Chem.* **2004**, *689*, 4083-4091.
(11) Labinger, J. A. *J. Mol. Catal. A: Chem.* **2004**, *220*, 27-35.
(12) Conley, B. L.; Tenn III, W. J.; Young, K. J. H.; Ganesh, S. K.; Meier, S. K.; Ziatdinov, V. R.; Mironov, O.; Oxgaard, J.; Gonzales, J.; Goddard III, W. A.; Periana, R. A. *J. Mol. Catal. A: Chem.* **2006**, *251*, 8-23.
(13) Periana, R. A.; Taube, D. J.; Gamble, S.; Taube, H.; Satoh, T.; Fujii, H. *Science* **1998**, *280*, 560-564.
(14) Grice, K. A.; Goldberg, K. I. *Organometallics* **2009**, *28*, 953-955.
(15) Stahl, S. S. *Angew. Chem. , Int. Ed.* **2004**, *43*, 3400-3420.
(16) Webb, J. R.; Bolaño, T.; Gunnoe, T. B. *ChemSusChem* **2011**, *4*, 1-1.
(17) Gonzales, J. M.; Distasio, R.; Periana, R. A.; Goddard, W. A.; Oxgaard, J. *J. Am. Chem. Soc.* **2007**, *129*, 15794-15804.
(18) Bischof, S. M.; Cheng, M.; Nielsen, R. J.; Gunnoe, T. B.; Goddard, W. A.; Periana, R. A. *Organometallics* **2011**, *30*, 2079-2082.
(19) Pouy, M. J.; Milczek, E. M.; Figg, T. M.; Otten, B. M.; Prince, B. M.; Gunnoe, T. B.; Cundari, T. R.; Groves, J. T. *J. Am. Chem. Soc.* **2012**, *134*, 12920-12923.
(20) Vaughan, G. A.; Rupert, P. B.; Hillhouse, G. L. *J. Am. Chem. Soc.* **1987**, *109*, 5538-5539.
(21) Van Asselt, A.; Trimmer, M. S.; Henling, L. M.; Bercaw, J. E. *J. Am. Chem. Soc.* **1988**, *110*, 8254-8255.
(22) Kays (nee Coombs), Deborah L.; Cowley, A. R. *Chem. Commun.* **2007**, 1053-1055.
(23) Conley, B. L.; Ganesh, S. K.; Gonzales, J. M.; Tenn, W. J.; Young, K. J. H.; Oxgaard, J.; Goddard, W. A.; Periana, R. A. *J. Am. Chem. Soc.* **2006**, *128*, 9018-9019.
(24) Ni, C.; Power, P. P. *Chem. Commun.* **2009**, 5543-5545.
(25) Figg, T. M.; Webb, J. R.; Cundari, T. R.; Gunnoe, T. B. *J. Am. Chem. Soc.* **2012**, *134*, 2332-2339.
(26) Prince, B. M.; Cundari, T. R. *Organometallics* **2012**, *31*, 1042-1048.
(27) Jeffrey, J. C.; Rauchfuss, T. B. *Inorg. Chem.* **1979**, *18*, 2658-2666.
(28) Braunstein, P.; Naud, F. *Angew. Chem. Int. Ed.* **2001**, *40*, 680-699.
(29) Bader, A.; Lindner, E. *Coord. Chem. Rev.* **1991**, *108*, 27-110.
(30) van der Boom, Milko, E.; Milstein, D. *Chem. Rev.* **2003**, *103*, 1759-1792.
(31) Komiya, S. *Coord. Chem. Rev.* **2012**, *256*, 556-573.
(32) Webb, J. R.; Burgess, S. A.; Cundari, T. R.; Gunnoe, T. B. *Dalton Trans.* **2013**, *42*, 16646-16665.
(33) Frisch, M. J. et al. GAUSSIAN 09 GAUSSIAN 09. **2009**, *Revision A.02; Gaussian Inc., Wallingford, CT, 2009*.
(34) Becke, A. D. *J. Chem. Phys.* **1988**, *88*, 1053-1062.
(35) Becke, A. D. *J. Chem. Phys.* **1993**, *98*, 5648-5652.
(36) Lee, C.; Yang, W.; Parr, R. G. *Phys. Rev. B* **1988**, *37*, 785-789.
(37) Stevens, W. J.; Krauss, M.; Basch, H.; Jasien, P. G. *Can. J. Chem.* **1992**, *70*, 612-630.
(38) Takano, Y.; Houk, K. N. *J. Chem. Theory Comput. ,* **2005**, *1*, 70-77.
(39) Ramírez, A.; Collum, D. B. *J. Am. Chem. Soc.* **1999**, *121*, 11114-11121.
(40) Lindner, E.; Wang, Q.; Mayer, H. A.; Fawzi, R.; Steimann, M. *Organometallics* **1993**, *12*, 1865-1870.
(41) Lindner, E.; Haustein, M.; Fawzi, R.; Steimann, M.; Wegner, P. *Organometallics* **1994**, *13*, 5021-5029.
(42) Figg, T. M.; Cundari, T. R.; Gunnoe, T. B. *Organometallics* **2011**, *30*, 3779-3785.
(43) Conley, B. L.; Ganesh, S. K.; Gonzales, J. M.; Tenn, W. J.; Young, K. J. H.; Oxgaard, J.; Goddard, W. A.; Periana, R. A. *J. Am. Chem. Soc.* **2006**, *128*, 9018-9019.
(44) Fang, X.; Scott, B. L.; Watkin, J. G.; Kubas, G. J. *Organometallics* **2000**, *19*, 4193-4195.
(45) Anderson, G. K.; Corey, E. R.; Kumar, R. *Inorg. Chem.* **1987**, *26*, 97-100.
(46) Thomas, J. C.; Peters, J. C. *J. Am. Chem. Soc.* **2001**, *123*, 5100-5101.
(47) Wehman, E.; Van Koten, G.; Knaap, C. T.; Ossor, H.; Pfeffer, M.; Spek, A. L. *Inorg. Chem.* **1988**, *27*, 4409-4417.
(48) Felicissimo, M. P.; Batista, A. A.; Ferreira, A. G.; Ellena, J.; Castellano, E. E. *Polyhedron* **2005**, *24*, 1063-1070.
(49) Figg, T. M.; Cundari, T. R. *Organometallics* **2012**, *31*, 4998-5004.
(50) Harrold, N. D.; Waterman, R.; Hillhouse, G. L.; Cundari, T. R. *J. Am. Chem. Soc.* **2009**, *131*, 12872-12873.
(51) Tolman, W., B. *Angew. Chem. Int. Ed.* **2010**, *49*, 1018-1024.
(52) Matsunaga, P. T.; Mavropoulos, J. C.; Hillhouse, G. L. *Polyhedron* **1995**, *14*, 175-185.
(53) Matsunaga, P. T.; Hillhouse, G. L.; Rheingold, A. L. *J. Am. Chem. Soc.* **1993**, *115*, 2075-2077.
(54) Alsters, P. L.; Teunissen, H. T.; Boersma, J.; Spek, A. L.; van Koten, G. *Organometallics* **1993**, *12*, 4691-4696.
(55) Kamaraj, K.; Bandyopadhyay, D. *Organometallics* **1999**, *18*, 438-446.

Table of Contents graphic